Correlation of Material and Processing Time Scales with Structure Development in Isotactic Polypropylene Crystallization

Aadil Elmoumni, H. Henning Winter,* and Alan J. Waddon

Department of Chemical Engineering and Department of Polymer Science and Engineering, University of Massachusetts, Amherst, Massachusetts 01003

Hitesh Fruitwala

Baytown Polymers Center, ExxonMobil Chemical Company, 5200 Bayway Drive, Baytown, Texas 77522

Received December 11, 2002; Revised Manuscript Received June 18, 2003

ABSTRACT: The influence of average molar mass and shear on the crystallization of isotactic polypropylene (*i*PP) has been studied. The Weissenberg number, a dimensionless parameter consisting of the product of the shear rate and a characteristic relaxation time ($\dot{\gamma}_0\lambda_r$), provides a criterion to locate the morphological transition from spherulitic to extended growth. The Weissenberg criterion applies to polymers of high and of low molecular weight. This is attributed to the importance of the initial nucleation process. Comparison of materials of different molar masses and various shear histories is allowed by the introduction of the normalized crystallization time τ, which is the ratio of the experimental time and a characteristic crystallization time λ_{Vvmax} that needs to be defined from the several possible choices. Rheological and rheooptical experiments furnish the material characteristic relaxation and crystallization time scales, respectively. The time λ_{Vvmax}, defined with light scattering as the moment at maximum density fluctuation invariant Q_η, is chosen here as a characteristic crystallization time scale since it is especially sensitive to the early stages of crystal growth that are responsible for the liquid-to-solid transition. DSC and WAXD have been used to further analyze the effect of shear on the populations of crystalline fractions present in the cooled *i*PP samples.

1. Introduction

Polymer molecules self-assemble during crystallization into nonequilibrium structures that depend on the time−temperature−strain history in complicated ways. Here we specifically focus on the way in which high molar mass of a polymer affects its crystallization. Several competing effects at different intrinsic time scales make quantitative predictions difficult. In *quiescent* crystallization, higher molecular weights will slow down the crystal formation because large molecules move more slowly. However, large molecules will connect crystalline regions over larger distances and thus facilitate long-range connectivity earlier, even though the overall crystallinity may still be relatively low. Under *shear*, the higher molecular weights can build higher stress and will retain orientation for a longer time. Higher orientation increases the molecular size (coil−stretching), lowers the entropy, and prepares for the ordered crystal morphology. Ordered regions serve as nuclei for the crystallization and, if the order is high enough, lead to global anisotropic crystal growth.

Under sufficiently high strains shish-kebab morphology can be created,[1] where highly stretched chains (shish) serve as nuclei[2] for the crystal formation of chain-folded lamellae overgrowths (kebab). According to Keller and Kolnaar,[1] chain extension enhances crystallization for two reasons. First, the extended chain is closer to its final configuration state in a crystal and has, therefore, a lower kinetic barrier to overcome than a random coil chain. Second, flow-induced orientation increases the melting temperature of the material and hence accelerates crystallization due to lower melt entropy of an extended chain compared to a random coil. Eder et al.[11] estimated this entropy change by dividing the first normal stress difference, which in a rubberlike liquid represents the stored free energy, by the absolute temperature. According to this estimate, Crystallization is only slightly enhanced by this second phenomenon.

Strain effects become dominant in polymers of high molecular weight.[1−6] An important parameter is the characteristic relaxation time λ_r (of the molten *i*PP), which increases with molecular weight. For studying the effect of shear on crystallization, a short term shearing is introduced as soon as the crystallization temperature is reached and before crystallization becomes observable.[3,7−12] The sheared state is characterized by increased molecular order that will last longer for higher molecular weights, due to a decreased rate of relaxation ($\sim e^{-t/\lambda_r}$), and thus anisotropic growth is expected to prevail longer.

A model material for quantifying these phenomena is isotactic polypropylene. Its main advantages are that it crystallizes slowly even at large supercooling, ΔT, below its melting temperature. Also, the number density of nuclei is low so that individual spherulites can grow to large size ($\sim$0.5 μm) before they begin to touch each other. This permits direct observation with an optical microscope. Strain at the onset of crystallization, in a sample that was cooled from the melt by some ΔT below T_m, increases the density of nuclei by orders of magnitude[13,14] and results in anisotropic crystal growth.

The aim of this work is to correlate the molecular time scales, namely the characteristic relaxation and crystallization times, with the morphological structures that arise upon application of shear at the onset of isotactic polypropylene's isothermal crystallization. Rheological

* Corresponding author. E-mail winter@ecs.umass.edu.

10.1021/ma025948n CCC: $25.00
Published on Web 07/30/2003

Table 1. Characteristics of Samples Utilized To Study the Effects of Molar Mass and Shear on the Crystallization of *i*PP[a]

sample	M_w (kg/mol)	M_n (kg/mol)	M_w/M_n	λ_i, s	λ_η, s	λ_η/λ_i
iPP171	171	40.4	4.2	5.50×10^{-2}	4.56×10^{-1}	8.20
iPP300	300	51.8	5.8	2.17×10^{-1}	1.54	7.10
iPP350	350	85.8	4.1	6.30×10^{-1}	4.76	7.94

[a] Characteristic relaxation times of *i*PP samples at 145 °C; λ_i: crossover from terminal behavior to entanglement. λ_η: crossover in steady-state shear viscosity curve from a plateau in η to the shear-thinning region.

and rheooptical experiments have been performed to obtain the characteristic time scales. Morphological changes during the quiescent and shear-induced isothermal crystallization have been monitored with optical microscopy. Results of this set of experiments have been merged to identify the effects of both molar mass and shear on the crystallization of isotactic polypropylene. Wide-angle X-ray diffraction (WAXD) and differential scanning calorimetry (DSC) have provided insight on the crystalline populations present in the cooled samples after completion of crystallization.

For this purpose, we first define the characteristic time scales of the crystallization experiment and then apply these in search for patterns in the data. Model experiments have been designed to guide this search. The potential benefit of the study is the merging of many phenomena into a unified pattern that becomes the basis for a predictive tool for polymer engineering.

Characteristic Time Scales. The developing structure in a crystallizing polymer is far away from equilibrium conditions. The immobile crystal structure arrests intermediate states that depend on temperature and flow history. Their characteristic time scales govern competing processes. The time scales involved can be grouped into (at least) three types that first need to be defined and then compared. These are the rheological relaxation time scale, the growth time of the crystalline structure, and the shearing time scales.

Rheological Time Scale, λ_r. Relaxation processes in the melt are typically scaled with the longest relaxation time. For a narrow distribution of molecular weight, this longest relaxation time appears as a cutoff in the relaxation time spectrum.[15] A clear definition exists for the longest relaxation time; it is the disengagement time of the macromolecules.[16] This results in a narrow crossover from entanglement behavior to the long-time behavior (terminal region of relaxation time spectrum). The broad distribution of molecular sizes in commercial polymers, however, broadens the crossover, and the definition of λ_{max} is commonly replaced by some average over the slow modes of the spectrum. For lack of a more specific time constant, rheologists often define a representative longest relaxation time with the intersect frequency ω_i at which dynamic moduli G' and G'' intersect (subscript "i" for intersect) in mechanical spectroscopy or by the onset of shear thinning at a characteristic shear rate $\dot{\gamma}_c$ in a steady shear experiment:

$$\lambda_i = \frac{1}{\omega_i} \quad \text{or} \quad \lambda_\eta = \frac{1}{|\dot{\gamma}_c|} \tag{1}$$

For our samples, these two time scales are proportional, separated by a common factor of about 8 (see Table 1). We selected $1/\omega_i$ as representative rheological time scale λ_r. Some justification for this procedure may be drawn from knowledge of narrowly distributed polymers for which the disengagement time is a fixed multiple of the intersect time[17]

$$\lambda_{max} = \alpha\left(\frac{1}{\omega_i}\right) \tag{2}$$

with α being a constant that is inherent to the polymer.

A second rheological time, the relaxation time near the transition to glassy behavior (Rouse time), is of no importance here, since the polyolefins of this study crystallize at temperatures much above the glass transition temperature, T_g. For polymers that crystallize near T_g, the Rouse time would need to be considered as additional parameter of possible importance.

Time Scale of Crystal Growth. It can be defined in many different ways depending on the type of observation (calorimetry, rheological, optical). Specific experiments probe the crystal structure in different ways and, hence, offer their own characteristic time scale. The most commonly used ones are the following:

Crystallinity: Calorimetry data (DSC) are often evaluated in terms of crystallization half-time $t_{1/2}$[18] or the Avrami time t_A.[19] At the crystallization half-time, $t_{1/2}$, the crystal fraction has reached half its final value. At the Avrami time, t_A, the relative degree of crystallinity has reached $X/X_\infty = 1 - e^{-1} = 0.63$, i.e., 63% of the final degree of crystallinity X_∞. The Avrami time is preferable because it assigns better physical meaning to the parameters in the Avrami fit of the data. DSC time constants relate to the later stages of crystallization (50% or 63%).

Analyses of crystallization using Avrami kinetics are based on the notion of growth of a spherulite from a central nucleus and assume that the nature of the material behind the growth front does not change with time. What actually happens is that the boundary of the spherulite is defined by the growth of its radial arms but also a considerable degree of crystallization occurs well behind the spherulite boundary between the radial arms. Optical microscopy images the advance of the growth front (ignoring the secondary crystallization effects) and can be treated by Avrami kinetics. In comparison, DSC exotherms measure the total crystallinity (including that behind the advancing growth front) and, if there is appreciable secondary crystallization, will not fit to Avrami kinetics. The Avrami model for crystallization is no longer widely used.

Effect of Crystal Growth on Rheological Behavior: Molecular motions correlate over larger and larger distances as the crystal structure grows. Relaxation processes slow down and pass through a unique rheological behavior at the gel point, which is associated with connectivity through the sample.[20−22] The critical gel (polymer at the gel point) is characterized by a self-similar relaxation modulus at long times[23]

$$G = S_c t^{-n_c} \quad \text{for} \quad t > \lambda_0 \tag{3}$$

S_c is the gel stiffness, n_c is the critical relaxation exponent, and λ_0 is the relaxation time denoting the crossover to some faster dynamics (entanglements, segmental dynamics). The gel time t_{gel} is defined as the time needed for a polymer to reach the critical gel state. It can be measured by small-amplitude oscillatory shear (SAOS) at low frequencies. In oscillatory shear the

dynamic moduli at the gel point also follow power law behavior

$$G' = \frac{G''}{\tan \delta} = S\Gamma(1 - n) \cos \frac{n\pi}{2} \omega^n \quad \text{for } \omega < 1/\lambda_0 \quad (4)$$

A consequence of power-law dynamics is a frequency-independent loss tangent

$$\tan \delta_c = \frac{G''}{G'} = \tan \frac{n\pi}{2} = \text{const} \quad \text{for } \omega < 1/\lambda_0 \quad (5)$$

This provides the most reliable and generally valid method for determining the gel time and the parameters n_c and S_c in crystallizing polymers.

Effect of Crystal Growth on Optical Properties: Optical properties are changing rapidly at early development of crystal structure. They are especially advantageous for our current study that focuses on this early development. Crystallization kinetics can be conveniently described in terms of the small-angle light scattering (SALS) invariants Q_δ and Q_η,[24] which are defined as integrated scattering intensities[25,26] along a line (i.e., along scattering vector).

$$Q_\delta = \int I_{Hv} q^2 \, dq = \frac{2\pi^2}{15}\left(\frac{\omega}{c}\right)^4 \langle \delta_n{}^2 \rangle \quad (6)$$

$$Q_\eta = \int \left(I_{Vv} - \frac{4}{3} I_{Hv}\right) q^2 \, dq = 2\pi^2 \left(\frac{\omega}{c}\right)^4 \langle \eta^2 \rangle \quad (7)$$

where I_{Vv} and I_{Hv} are the polarized and depolarized scattering intensities, $q = (4\pi/\lambda) \sin(\theta/2)$ is the scattering vector, ω is the angular frequency, c is the speed of light in a vacuum, $\langle \delta_n{}^2 \rangle$ is the mean-square orientation fluctuation, and $\langle \eta^2 \rangle$ is the mean-square density fluctuation. Hence, Q_η is analogous to the mean-square density fluctuations $\langle \eta^2 \rangle$ and Q_δ parallels orientation fluctuations, i.e., mean-square optical anisotropy $\langle \delta_n{}^2 \rangle$.

SALS provides several possible characteristic crystallization time scales for describing the early growth of crystal structure: (a) the inverse slope $(\partial(Q_\delta/Q_\delta{}^\infty)/\partial t)^{-1} = \lambda_{Hvmax}$ of the normalized orientation fluctuation invariant $Q_\delta/Q_\delta{}^\infty$ at the crystallization half-time, (b) the inverse slope of the growing density fluctuation invariant Q_η at the early stages of the crystallization, or (c) the instant of maximum in the density fluctuation invariant, λ_{Vvmax}.

Turbidity increases strongly during crystal growth.[7,27,29] A characteristic time for crystal growth is the turbidity half-time t_τ, the time at which the normalized transmitted intensity has decayed to half its initial value.[29] t_τ as experimental parameter is appealing since transmission is easy to measure, even in oriented samples and/or in samples with gradients in crystallinity.

These optical time scales are affected differently by the crystal growth. Typically, one finds λ_{Vvmax} to be about half the turbidity half-time while λ_{Hvmax} is slightly lower than t_τ:

$$\lambda_{Vvmax} < \lambda_{Hvmax} < t_\tau \quad (8)$$

Since we were especially concerned with the early stages of crystallization, we chose λ_{Vvmax} as characteristic crystallization time.

Shear Flow Time Scales. The applied shear flow is characterized by its short duration, Δt_s, and by a constant (about) shear rate of magnitude, $\dot{\gamma}_0$. This provides two time scales for quantifying the effects of shear: the shearing time Δt_s and the inverse of the shear rate $1/\dot{\gamma}_0$. $|1/\dot{\gamma}_0|$ is the time needed to introduce a shear strain of $\gamma = 1$ into the sample, and $(\Delta t_s \dot{\gamma}_0)$ is the total strain of the short shearing process that precedes crystallization. For flow-induced molecular orientation, not only does the strain rate need to exceed a critical value, but the total strain must also exceed a critical value. In our experiments, however, the applied total strains were always large enough for the second criterion to be satisfied, and so only strain rate effects were pertinent.

Dimensionless Groups. The ratio of these time scales allows comparison of the competing processes. This leads to the set of dimensionless groups for evaluating the range of our experiments:

The Weissenberg Number We $(=\dot{\gamma}_0 \lambda_r)$: The effect of strain on crystal growth is expected to depend on the extent of flow-induced orientation and the rate at which this orientation relaxes. If the strain is imposed at low rate, $We < 1$, then flow-induced molecular conformations can relax and crystal growth is expected to be random while the nucleation density may already be increased. For higher strain rates, $We > 1$, where the melt is oriented, nucleation is drastically increased, and crystal growth is anisotropic, at least in its initial phase. The value of *We* is an important parameter of our experiments, which needs to be explored in greater detail. It might lend itself to unite the shear-crystallization phenomena into a more general pattern that will serve as a prognostic tool for polymer engineering.

Normalized Crystallization Time τ $(\tau = t/\lambda_x)$: Defined as the ratio of the experimental time with the characteristic crystallization time, τ enables comparison of morphological differences between quiescent and shear-induced crystallization. This allows for a collection of snapshots of the evolution of crystal growth at increased effects of shear.

Ratio Gel Time/Crystallization Time: In the case of quiescent crystallization, two ongoing processes dominate crystal growth. First, the formation of aggregates and fibrous "strands" governed by radial growth rate. This process is responsible for interconnected network formation (gelation) and is manifested experimentally in t_{gel}. Second, the internal crystallization inside the aggregates (through making them volume-filled with ordered crystals) governed by internal crystallization rates. This process is responsible for the growth of crystallinity and is manifested experimentally through t_A. If the radial growth is dominating (high radial growth rate, short t_{gel}), the crystallinity at GP will be lower (small values of t_{gel}/t_A) and vice versa. The competition of these processes may be evaluated from the dimensionless group t_{gel}/t_A.

Ratio Crystallization Time/Shearing Time $(=\lambda_x/\Delta t_s)$: A large ratio $\lambda_x/\Delta t_s$, with λ_x being a characteristic crystallization time, means that the shearing action has been completed before substantial amounts of crystal have developed. If, however, this ratio is small, then growing crystal structures are subjected to shear flow and shear-induced deformation. For our model experiments, this ratio is large while it is typically small for polymer processing.

Ratio of Rheological Time to Crystallization Time (λ_r/λ_x): A large value means that the molecules remain in an equilibrium state during the early stages of crystallization. If crystallization occurs much faster

than relaxation, then crystallization might introduce stress. This is an option that should be explored.

Dimensionless groups for time scales for crystallization and for rheology are interrelated as

$$\lambda_x \dot{\gamma}_0 = \frac{\lambda_x}{\lambda_r} \lambda_r \dot{\gamma}_0 = \frac{\lambda_x}{\lambda_r} We \tag{9}$$

As a working hypothesis, we assume that the dimensionless groups as defined above provide a framework for studying the phenomena and consequences of shear-induced crystallization.

2. Experimental Section

Materials. Three commercial grades of isotactic polypropylene (*i*PP) (of ExxonMobil) with various molecular weights (M_w) were used (see Table 1). The samples were melted at 200 °C for 10 min to erase previous shearing histories, then cooled to the experimental temperature, $T_x = 145$ °C (below T_m), and held there for isothermal crystallization directly in the rheometer (to investigate the stiffening of the crystallizing structure) or in the Linkam hot-stage (to monitor the structure growth with optical microscopy and SALS). The actual rheological or optical experiment was started as soon as the experimental temperature was reached. For shear-induced crystallization experiments, a total shear strain $\gamma = 600$ was applied to the samples as soon as T_x was reached. X-ray and DSC experiments on cooled samples gave information about the final state.

Techniques and Instruments. The rheological experiments were performed on crystallizing samples using the time-resolved rheometry technique[30] with a rotational rheometer (Stresstech of ATS RheoSystems) equipped with cone−plate fixtures (diameter 25 mm, 4° angle).

(SAOS) was started as soon as the experimental temperature was reached. Cyclic frequency sweeps (CFS) were performed repeatedly in the frequency window between 0.01 and 10 rad/s (5 points per decade). The shear strain amplitude was 0.04, which ensured sufficiently high torque values while remaining in the linear viscoelastic range.

Growing spherulites and threads were observed under a universal polarizing microscope (Carl Zeiss, model ZPU01). SALS was measured in a self-built rheooptical setup[12] and analyzed with a newly written program (LabVIEW based). Both the microscope and rheooptical SALS setup were equipped with a shearing hot-stage (CSS 450 of Linkam Scientific Instruments). A disk-shaped sample is held between concentric disks with a gap of 200 μm. The shear rate increases linearly with distance from the center; however, the shear rate is approximately constant in the light path, which is normal to the disk. Three shear rates were selected: $\dot{\gamma} = 1$, 5, and 10 s^{-1} (at the radial position of the window of the Linkam device).

The final *i*PP structure formed was evaluated with WAXD using a flat plate Statton camera with Ni-filtered Cu Kα radiation. Samples were heated from room temperature to 200 °C at a rate of 5 K/min in a differential scanning calorimeter (Q1000 of TA Instruments) to obtain thermograms.

3. Results

Rheology. Characteristic relaxation times λ_i, obtained from the intersect of G' and G'', were determined from frequency-dependent data at temperatures between 140 and 220 °C, which were superimposed (by simultaneous horizontal and vertical shifting) to yield master curves at a reference temperature $T_{ref} = 145$ °C (the experimental crystallization temperature). The superposition plots of storage and loss moduli are shown in Figure 1. Characteristic relaxation times λ_i are summarized in Table 1. λ_i increases with increasing molecular weight (see Figure 3, circles). A line of slope

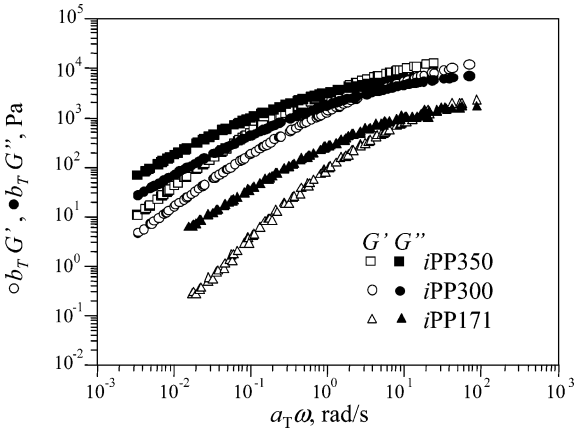

Figure 1. Melt rheology of *i*PP samples. Storage modulus G' and loss modulus G'' of *i*PP samples shifted to 145 °C.

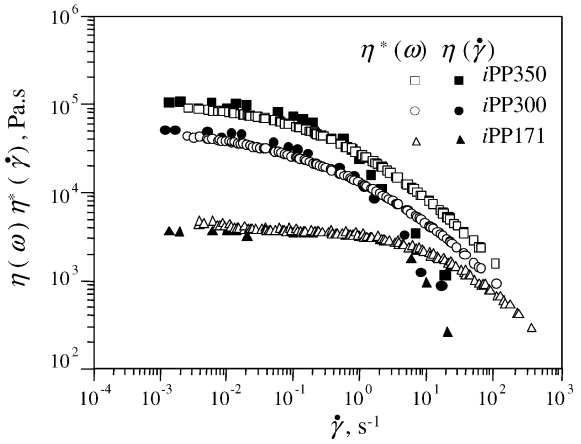

Figure 2. Shear viscosity as a function of shear rate at 145 °C along with dynamic viscosity curves from time−temperature superposition shifted to 145 °C. Crossover from zero shear viscosity η to shear thinning region gives characteristic relaxation time λ_η. High shear rate data are affected by slip phenomena and fall below predictions from the Cox−Merz relation.

3.4 (denoting the expected relationship $\lambda_r \sim M_w^{3.4}$) is drawn into Figure 3 for comparison.

Relaxation times λ_η denoting the onset of shear thinning in the steady-state shear viscosity were obtained from steady shear experiments of the *i*PP melt performed at $T = 220$ °C under a nitrogen environment (see Table 1 and Figure 3, triangles). Figure 2 shows the shifted shear viscosity values (to 145 °C using the shift factors obtained from the dynamic data) in a range of shear rates between 10^{-3} and 20 s^{-1} together with shifted (to 145 °C) dynamic viscosity data obtained from time−temperature superposition. The zero-shear viscosity η_0 was obtained at low shear rates and plotted vs molecular weight in Figure 3 (squares).

Figure 4 compares the observed t_{gel} for quiescent and shear-induced crystallization at $T_x = 145$ °C. We observe a higher t_{gel} with increasing M_w in the case of quiescent crystallization. If shear is applied to samples prior to crystallization, t_{gel} shortens significantly, especially for the higher molar mass samples.

Small-Angle Light Scattering. Figure 5 shows the evolution of SALS invariants Q_η and Q_δ of *i*PP350 at various shearing conditions. Density fluctuations (filled symbols) appear at the very early times, pass through a maximum, and decrease at later stages when the crystalline phase becomes dominant. The intensity

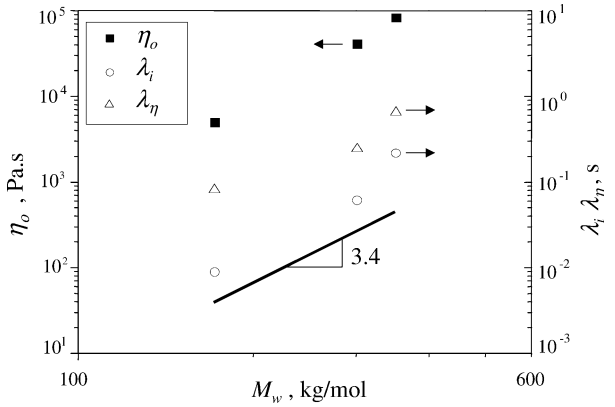

Figure 3. Zero-shear viscosity and characteristic relaxation times vs molecular weight.

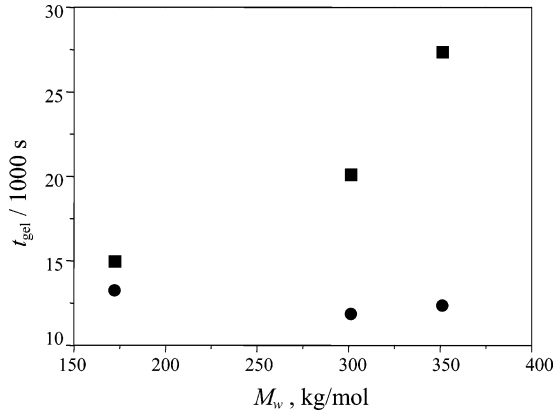

Figure 4. Liquid-to-solid transition of *i*PP samples (gel time) as a function of molecular weight at 145 °C. The temperature history was the same for all samples, rapid cooling from 200 to 145 °C. Quiescent crystallization in black squares (■); sheared samples (shear rate of 10 s^{-1}, $t_s = 60$ s) in full circles (●).

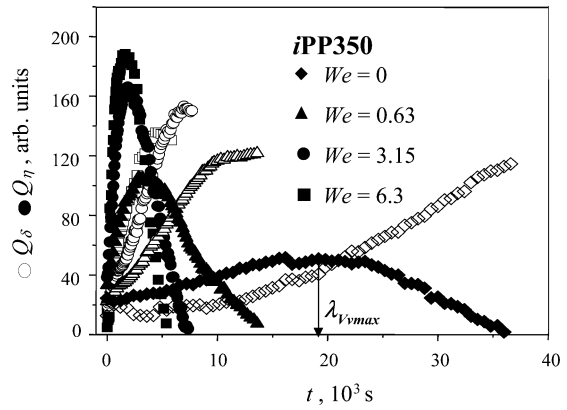

Figure 5. Time evolution of SALS invariants Q_η and Q_δ of *i*PP samples, quiescent and sheared ($\dot\gamma = 1$, 5, and 10 s^{-1}, with $t_s = 600$, 120, and 60, respectively), at increasing *We* values. λ_{Vvmax} is crystallization time corresponding to instant at maximum density fluctuations. Density fluctuation invariant Q_η in full symbols and orientation fluctuation invariant Q_δ in open symbols.

maximum is reached earlier if more shear is introduced to the samples. The orientation fluctuations (hollow symbols), due to optical anisotropy of crystals, develop at much later stages and show sigmoidal growth. Full intensity values are reached earlier as more shear is applied.

Characteristic crystallization times λ_{Vvmax}, defined as the instant at maximum density fluctuations invariant

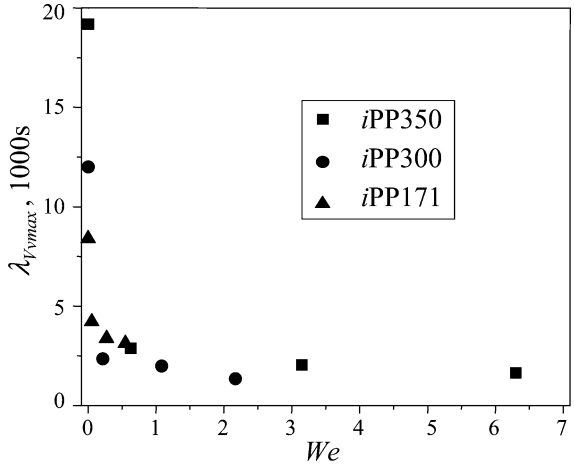

Figure 6. Characteristic crystallization time λ_{Vvmax} vs Weissenberg number for all molar mass samples.

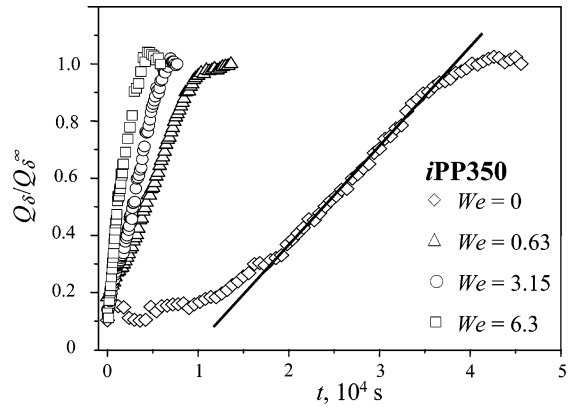

Figure 7. Reduced orientation fluctuations Q_δ/Q_δ^∞ for *i*PP350 showing linear fit at crystallization half-time.

Q_η, were obtained from data such as in Figure 5. We observe a decrease in λ_{Vvmax} with increasing shear rate; this is expected since orientation enhances crystallization hence reducing its time scale. A substantial increase in intensity at λ_{Vvmax} is also observed for each molar mass with increasing shear rate; this is attributed to the increased number density of scatterers (crystallites), which grow from nuclei created by the shear-induced orientation.

The effect of the Weissenberg number *We* on nucleation is shown in Figure 6. A sharp decrease in crystallization time λ_{Vvmax} occurs at low *We* values where isotropic scattering is dominant (*We* < 1, where spherulitic morphology is observed as will be discussed in the optical microscopy results) and then seems to reach an asymptotic value at higher values of *We* (*We* > 1, where shish-kebab morphology is seen). This phenomenon can be used as a criterion for identifying the transition from isotropic to anisotropic crystal growth.

Time variation of the normalized orientation fluctuations invariant Q_δ/Q_δ^∞ taken for *i*PP350 at increasing Weissenberg number values are shown in Figure 7. Q_δ^∞ is defined as the maximum value of the orientation fluctuation invariant at the late stages of the crystallization experiment. From the inverse slope $(\partial(Q_\delta/Q_\delta^\infty)/\partial t)_T$ of these curves we can estimate a characteristic crystallization time (λ_{Hvmax})[28] (see Figure 7). The slope $(\partial(Q_\delta/Q_\delta^\infty)/\partial t)_T$, which is regarded as a crystallization rate $(\lambda_{Hvmax})^{-1}$, is plotted against the Weissenberg number for all molar masses in Figure 8. The increase from *We* = 0 to *We* = 1 increases the crystallization rate

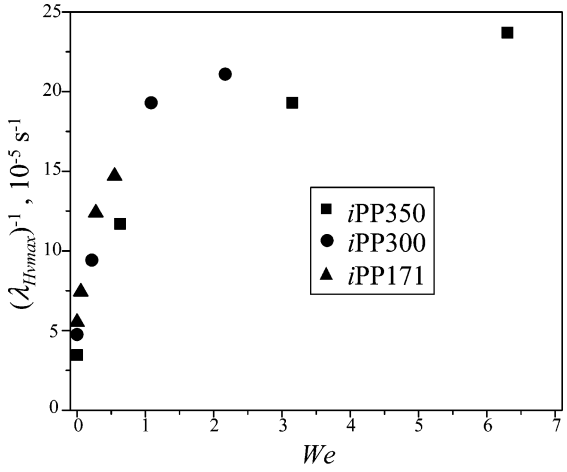

Figure 8. Reduced orientation fluctuation slopes of all molar mass samples at increasing Weissenberg values.

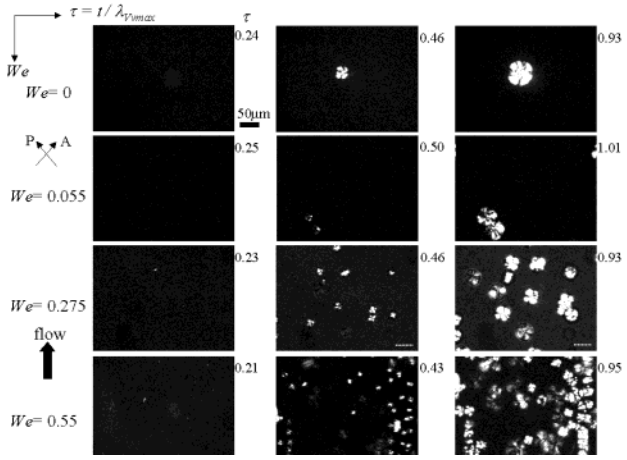

Figure 9. Optical micrographs showing evolution of quiescent and shear-induced crystallization of *i*PP171 at increasing *We* values. Micrographs shown at increasing normalized time scale $\tau = t/\lambda_{Vvmax}$ for comparison.

by about 3-fold; further increase of the Weissenberg number value seems to increase the alignment in the polymer while $(\lambda_{Hvmax})^{-1}$ is not substantially increased further.

Optical Microscopy. Optical micrographs of the samples at increasing *We* are shown in Figures 9 and 10. In quiescent crystallization, a small number of nuclei appear in the beginning, and their number stays constant from thereon. The crystal growth rate is uniform so that the radius $R(t)$ is practically the same for all spherulites. An increase in nucleus density[7] for all samples is observed as shear is applied prior to the isothermal crystallization. This phenomenon is more pronounced in the high molar mass samples where a transition from sporadic to row nuclei occurs. Indeed, as shown on the micrographs, the low molar mass sample *i*PP171 only shows a spherulitic structure to a *We* value of 0.55, while the high molar mass sample *i*PP300 shows a transition from spherulitic to shish-kebab structure at a *We* value of about 1 or higher.

Since the crystal growth rates of the quiescent and shear-induced crystallization are different, we introduced a dimensionless time scale τ, defined as the ratio of the experimental time with the characteristic crystallization time (λ_{Vvmax}) obtained from SALS results, to contrast the resulting morphologies. This enables us to compare crystallization of different materials subjected

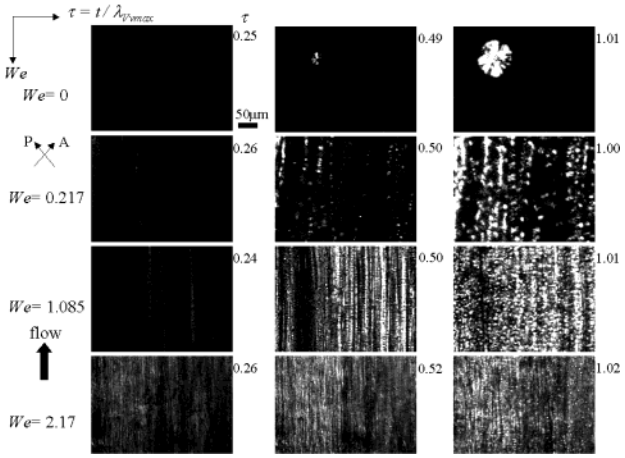

Figure 10. Optical micrographs showing evolution of quiescent and shear-induced crystallization of *i*PP300 at increasing *We* values. Micrographs shown at increasing normalized time scale $\tau = t/\lambda_{Vvmax}$ for comparison.

to different shear histories. Indeed, by comparing the micrographs in a column fashion in each Figures 9 and 10 at an equivalent normalized time τ, the effect of shear on nucleation and growth is uncovered. For sample *i*PP171, crystal growth is spherulitic up to a value *We* of 0.55 while nucleation density increases; the high molecular weight sample *i*PP300 can access higher *We* values (above 1 since the relaxation time λ_i is higher) where a transition to shish-kebab structure is seen.

Wide-Angle X-ray Diffraction. Wide-angle X-ray diffraction was performed on the cooled samples after completion of crystallization (see Figure 11). The monoclinic lattice structure[31] of isotactic polypropylene, with lattice constants $a = 6.6$ Å, $b = 20.78$ Å, $c = 6.5$ Å, and a tilt angle $\beta = 99.6°$, gives rise to the main reflections from the crystallographic planes (110), (040), (130), (111), and (041). The first three of these crystallographic planes are parallel to the chain axis, which can align with the flow direction. The patterns are composed of two composite patterns, each corresponding to (i) the chain extended fibrils aligned parallel to the flow direction and (ii) chain-folded lamellae (kebab) overgrowths that adopt a helical growth habit in a direction perpendicular to the nucleating fibril. In Figure 11, patterns of *i*PP300 and *i*PP171 at increased *We* were taken. The important features are the equatorial patterns of the (110) and (040) reflections observed at *We* about 1 and higher. These arise from the extended chain component in the structure. Because the chains are parallel to the flow axis, these planes are also parallel to the sample axis and therefore must reflect X-ray intensity at right angles to the flow direction. For sample *i*PP171, the reflections obtained are isotropic up to a *We* value of 0.55 and lead to the conclusion that no chain extended component is present. This is in accordance with optical studies shown above.

Differential Scanning Calorimetry. DSC thermograms show the difference in morphology of quiescent and sheared *i*PP samples, here at a heating rate of 5 K/min (Figures 12 and 13). We take advantage of the linear increase of the shear rate with radial position r/R. Sections of the sheared samples, corresponding to different *We* values, were cut, and thermograms were measured. The sheared samples melt with two peaks: one at a temperature ~171 °C that can be attributed to the melting of the chain extended component[32] and the

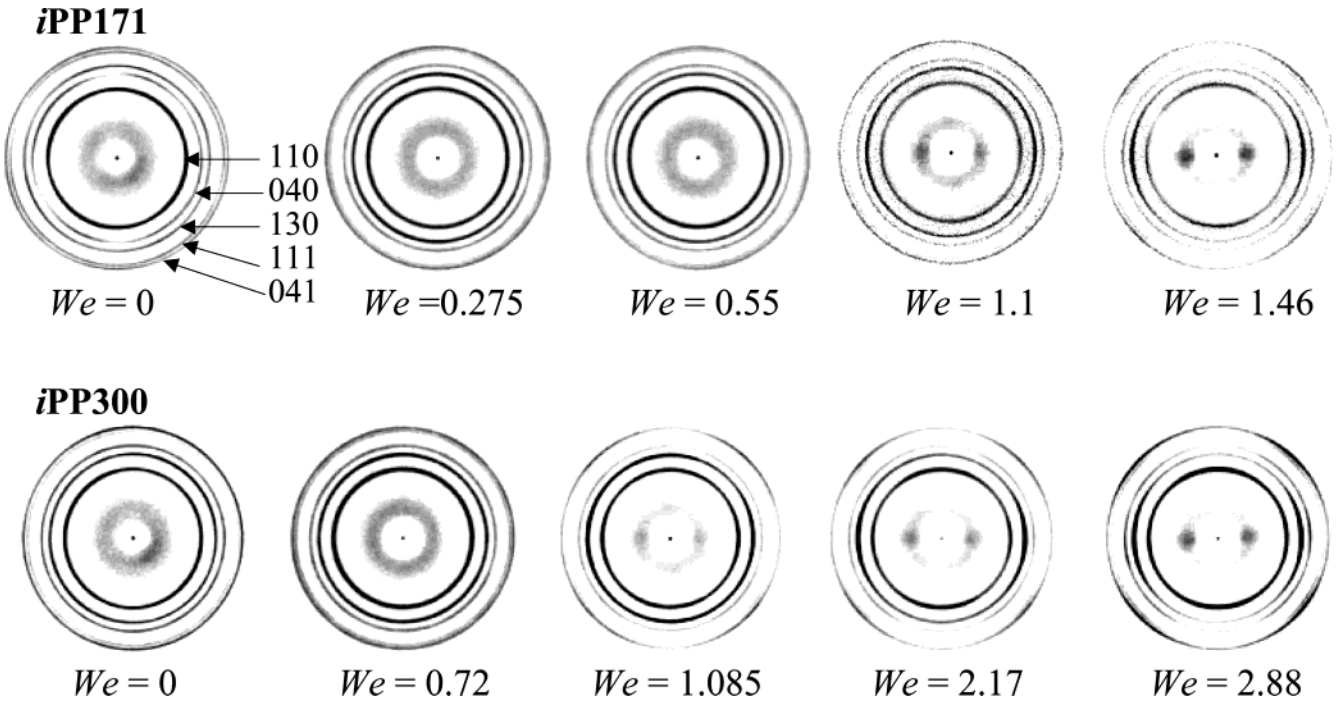

Figure 11. WAXD images of quiescent and shear-induced crystallization of *i*PP171 and *i*PP300 at increasing Weissenberg values. Arrows indicate various crystal planes of the α-polypropylene crystalline structure.

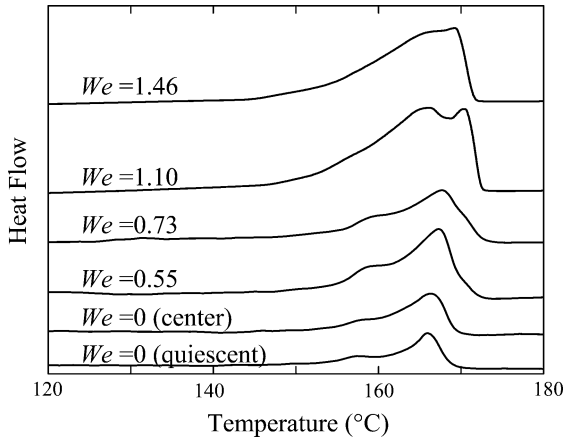

Figure 12. DSC thermograms of sections from quiescent and sheared samples of *i*PP171, at corresponding Weissenberg numbers, heated from room temperature to 200 °C at 5 K/min. The first curve at *We* = 0 corresponds to a section from a quiescently crystallized sample, while the second curve is of a section cut from the center of the shear crystallized sample corresponding to *We* = 0.

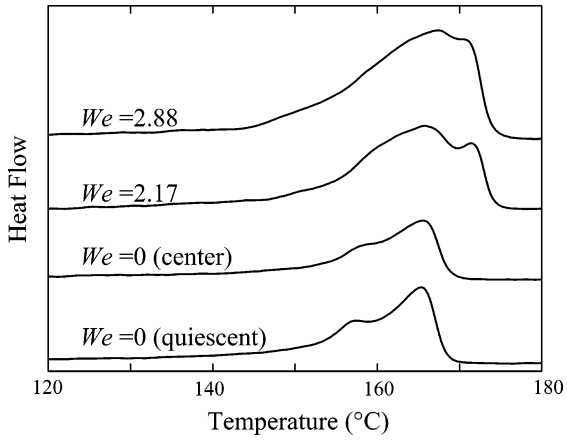

Figure 13. DSC thermograms of sections from quiescent and sheared samples of *i*PP300, at corresponding Weissenberg numbers, heated from room temperature to 200 °C at 5 K/min. The first curve at *We* = 0 corresponds to a section from a quiescently crystallized sample, while the second curve is of a section cut from the center of the shear crystallized sample corresponding to *We* = 0.

other around 166 °C corresponding to the nominal melting of the unoriented spherulites consisting of chain-folded lamellae. The extra peak is not present in the thermograms of the quiescent samples, the pieces cut from the center of the samples and sections that correspond to *We* values about and below 1. Thermograms of sample *i*PP171 sheared at an equivalent *We* of 0.55 do not show the extra peak in keeping with the results from optical and X-ray experiments, while the thermograms of an *i*PP171 sample sheared at *We* of 1.10 show the peak around ∼171 °C (see Figure 12).

4. Discussion

The Weissenberg number correlates shear effects in crystallizing *i*PP in remarkable ways. At first glance, this is not surprising since *We* = 1 (about) marks the onset of shear thinning in steady shear flow. This onset of shear thinning is attributed to the crossover from slow flow, in which equilibrium conformations are maintained, to fast flow with nonequilibrium conformations. Small deviations from equilibrium (near *We* = 1) already result in a drastic increase in nucleation density. Larger deviations result in anisotropic growth of crystal structure. Instead of spherulites, threadlike structures grow (shish-kebab morphology).

The surprising aspects of the correlation with *We* values are severalfold. The Weissenberg number is defined with melt states of the polymer. The shearing (rate $\dot{\gamma}$) occurs in the melt before crystallization becomes observable,[2] and the relaxation time λ_r belongs to the polymer in the molten state. However, the crystallization observations are made at a later time where characteristic times have changed already due to the

evolving molecular connectivity (by crystallization) and because of the lowering of the temperature.

The Weissenberg number does not capture the relaxation process that occurs after cessation of flow. A large *We* may be achieved with a large shear rate or a large relaxation time (large molecular weight), or both. However, relaxation depends on the magnitude of the relaxation time. A higher molecular weight polymer retains the shear-induced orientation for longer times. For this reason, in an experiment with the same *We*, the high molecular weight material should show much stronger shear effects on crystallization. However, differences are very small. This is quite surprising, and it tells us that relaxation is of little importance in our crystallization experiments. Previous results by Eder et al.[11] and Alfonso at al.[33] agree with this finding; in short shearing experiments with a box pressure−time profile (pressure driven flow), flow-induced birefringence appears quickly at the onset and disappears almost immediately when the flow stops. However, the effects on subsequent crystallization are large.

The correlation with *We* suggests that the shear influence is strongest at the very beginning of the crystallization process, i.e., during nucleation. Shearing not only increases the nucleation density but also introduces anisotropy into the nuclei that prevails during the subsequent growth. The shear-induced structure seems to be long-lived and independent of melt relaxation properties. A second reason for the lack of sensitivity to melt relaxation properties might be the rapid growth of connectivity in the polymer. Crystalline regions reduce the mobility of all molecules. Even low molecular weight samples cannot relax quickly anymore. The difference between small and large molecules is less pronounced and has less effect on the evolving crystal structure.

Suitable experiments need to be designed for exploring these hypotheses. The correlation with *We* remains a surprising result that, however, agrees with recent findings on poly-1-butene.[34]

The anisotropic crystallization after shearing at high *We* is followed by spherulitic overgrowth. Keller[1] has reported this phenomenon and attributed it to low molecular weight chains that can relax quickly. The overgrowth is large enough to be seen in the optical microscope[12] and is also found for the samples of this study.

In the analysis we assume that *We*, as defined with the crossover time, is proportional to a *We* defined with the absolute longest relaxation time (which is not known to us). All our observations would be shifted with such a redefinition of *We*, and nonlinearities would set in at a comparatively low *We* value. The shift is difficult to estimate, but it may be as large as 1 order of magnitude. The value of *We* is somewhat arbitrary since we do not know the longest relaxation time of our broadly distributed polymer. The crossover from flow behavior to elasticity-dominated behavior ("rubber plateau") occurs over a wide frequency (or time) range while data are quite limited for experimental reasons. The intersect time λ_i (inverse of frequency ω at which G' and G'' intersect) is a suitable reference in the vicinity of the longest relaxation time. The intersect time is appealing since it is clearly defined by the dynamic mechanical experiment.

The shear strain is purposely introduced while the polymer is in the melt state so that molecular conformations and the resulting stress−strain relations are governed by melt dynamics. This simplifies the data analysis and leads to a more clear understanding of the observations since distinct patterns can be detected in the behavior. It should be noted, however, that polymer processing with crystallization is a degree more complicated. Processing flows proceed beyond the initial short interval and continue during crystal growth.[35] In film blowing, the deformation continues until a semicrystalline structure that has grown sufficiently strong to arrest the flow. Fiber spinning flows proceed even further; strain is applied not only during the initial formation of the fiber but also at later stages where crystallinity has advanced significantly. Blow molding is another process that introduces large strains in the polymer near its crystallization threshold; the polymer temperature is typically brought close to the crystallization temperature when the strain is introduced in a rapid stretching process. These more complicated processes of crystal growth under flow are not addressed here.

5. Conclusion

The Weissenberg number is a suitable criterion for quantifying the effect of the shear flow on *i*PP crystallization. At very low *We*, quiescent crystallization dynamics prevail. At intermediate *We*, the nucleation rate is increased. The increase is rather large; however, crystal growth occurs in spherulites that do not look different from quiescently crystallizing spherulites (at least in the optical microscope). At higher *We*, the crystal growth is anisotropic at a large enough scale to be observable in an optical microscope. Higher molar mass samples can easily access the transition to shish-kebab structure since *We* is higher (greater relaxation time). Normalized crystallization time τ enables comparison of morphological differences between quiescently and shear-induced crystallized *i*PP samples. Micrograph examination at a chosen τ reveals the effect of shear on nucleation and growth of the crystallization process. Analysis of cooled sheared samples by WAXD shows a significant increase of molecular orientation along the *c* axis (which is the flow direction) with increasing *We*, demonstrated by the appearance of high-intensity arcs in the *hk*0 reflections. DSC thermograms also confirm the presence of two crystalline populations, where an extra melting peak (at about 171 °C) appears after the nominal melting peak of a quiescently crystallized isotactic polypropylene. Its area also rises with increasing *We*.

Acknowledgment. We thank ExxonMobil Co. and the National Science Foundation (NSF/CTS-0105156) for funding this project. We thank our co-workers Dr. Roland Horst and Souvik Nandi for their valuable work developing the software needed for performing the SALS experiments.

References and Notes

(1) Keller, A.; Kolnaar, H. W. Flow Induced Orientation and Structure Formation. In *Processing of Polymers;* Meijer, H. E. H., Ed.; VCH: New York, 1997; Vol. 18, pp 189−268.
(2) Seki, M.; Thurman, D. W.; Oberhauser, J. P.; Kornfield, A. J. *Macromolecules* **2002**, *35*, 2583−2594.
(3) Eder, G.; Janeschitz-Kriegl, H. Crystallization. In *Processing of Polymers*; Meijer, H. E. H., Ed.; VCH: New York, 1997; Vol. 18, pp 189−268.
(4) Jerschow, P.; Janeschitz-Kriegl, H. *Intern. Polym. Process. XII* **1997**, *1*, 72−77.

(5) Pennings, A. J.; Van der Mark, J. M. A. A.; Booij, H. C. *Kolloid Z. Z. Polym*. **1970**, *236*, 99−111.
(6) Goschel, U.; Swartjes, F. H. M.; Peters, G. W. M.; Meijer, H. E. H. *Polymer* **2000**, *41*, 1541−1550.
(7) Liedauer, S.; Eder, G.; Janeschitz-Kriegl, H.; Jerschow, P.; Geymayer, W.; Ingolic, E. *Int. Polym. Process.* **1993**, *8*, 236−250.
(8) Eder, G.; Janeschitz-Kriegl, H.; Krobath, G. *Prog. Colloid Polym. Sci.* **1989**, *80*, 1−7.
(9) Janeschitz-Kriegl, H. *Rheol. Fundam. Polym. Proc.* **1995**, 409−418.
(10) Janeschitz-Kriegl, H.; Eder, G. *J. Macromol. Sci., Chem.* **1990**, *A27*, 1733−1756.
(11) Eder, G.; Janeschitz-Kriegl, H.; Liedauer, S. *Prog. Polym. Sci.* **1990**, *15*, 629−714.
(12) Pogodina, N. V.; Lavrenko, V. P.; Srinivas, S.; Winter, H. H. *Polymer* **2001**, *42*, 9031−9043.
(13) Tribout, C.; Monasse, B.; Haudin, J. M. *Colloid Polym. Sci.* **1996**, *274*, 197−208.
(14) Lee, O.; Kamal, M. R. *Polym. Eng. Sci.* **1999**, *39*, 236−248.
(15) Baumgaertel, M.; Schausberger, A.; Winter, H. H. *Rheol. Acta* **1990**, *29*, 400−408.
(16) Doi, M.; Edwards, S. F. *The Theory of Polymer Dynamics*; Clarendon Press: Oxford, England, 1986.
(17) Carri, G. A.; Winter, H. H. *Rheol. Acta* **1997**, *36*, 330−344.
(18) Alfonso, G. C.; Ziabicki, A. *Colloid Polym. Sci.* **1995**, *273*, 317−323.
(19) Pogodina, N. V.; Siddiquee, S. K.; Van Egmond, J. W.; Winter, H. H. *Macromolecules* **1999**, *32*, 1167−1174.
(20) te Nijenhuis, K.; Winter, H. H. *Macromolecules* **1989**, *22*, 411−414.
(21) Lin, Y. G.; Mallin, D. T.; Chien, J. C. W.; Winter, H. H. *Macromolecules* **1991**, *24*, 850−854.
(22) Richtering, H. W.; Gagnon, K. D.; Lenz, R. W.; Fuller, R. C.; Winter, H. H. *Macromolecules* **1992**, *25*, 2429−2433.
(23) Winter, H. H.; Mours, M. *Adv. Polym. Sci.* **1997**, *134*, 165−234.
(24) Stein, R. S.; Wilson, P. R. *J. Appl. Phys.* **1962**, *33*, 1914−1920.
(25) Koberstein, J.; Russell, T. P.; Stein, R. S. *J. Polym. Sci., Polym. Phys. Ed.* **1979**, *17*, 1719−1730.
(26) Stein, R. S. *Rubber Chem. Technol.* **1976**, *49*, 458−535.
(27) Kumaraswamy, G.; Issaian, A. M.; Kornfield, J. A. *Macromolecules* **1999**, *32*, 7537−7547.
(28) Okamoto, M.; Kubo, H.; Kotaka, T. *Macromolecules* **1998**, *31*, 4223−4231.
(29) Acierno, S.; Grizzuti, N.; Winter, H. H. *Macromolecules* **2002**, *35*, 5043−5048.
(30) Mours, M.; Winter, H. H. *Rheol. Acta* **1994**, *33*, 385−397.
(31) Lotz, B.; Wittmann, J. C. *Polymer* **1996**, *37*, 4979−4992.
(32) Somani, R. H.; Yang, L.; Sics, L.; Hsiao, B. S.; Pogodina, N. V.; Winter, H. H.; Agarwal, P.; Fruitwala, H.; Tsou, A. *Macromol. Symp.* **2002**, *185*, 105−117.
(33) Ziabicki, A.; Alfonso, G. C. *Macromol. Symp.* **2002**, *185*, 211−231.
(34) Acierno, S.; Palomba, B.; Grizzuti, N.; Winter, H. H. *Rheol. Acta* **2003**, *42*, 243−250.
(35) Tadmor, Z.; Gogos, G. C. *Principals of Polymer Processing;* John Wiley & Sons: New York, 1979.

MA025948N